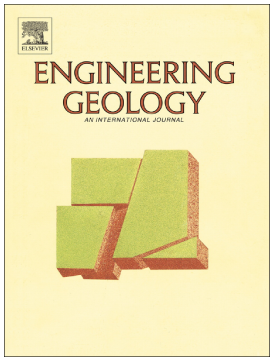

P-wave velocity measurements for preliminary assessments of the mineralization in seafloor massive sulfide mini-cores during drilling operations

Giovanni Spagnoli, Bradley A. Weymer, Marion Jegen, Erik Spangenberg, Sven Petersen

PII: S0013-7952(17)30552-5
DOI: doi: 10.1016/j.enggeo.2017.07.003
Reference: ENGEO 4600

To appear in: *Engineering Geology*

Received date: 6 April 2017
Revised date: 19 June 2017
Accepted date: 13 July 2017

Please cite this article as: Giovanni Spagnoli, Bradley A. Weymer, Marion Jegen, Erik Spangenberg, Sven Petersen , P-wave velocity measurements for preliminary assessments of the mineralization in seafloor massive sulfide mini-cores during drilling operations. The address for the corresponding author was captured as affiliation for all authors. Please check if appropriate. Engeo(2017), doi: 10.1016/j.enggeo.2017.07.003

P-wave velocity measurements for preliminary assessments of the mineralization in seafloor massive sulfide mini-cores during drilling operations

Giovanni Spagnoli[1], Bradley A. Weymer[2], Marion Jegen[2], Erik Spangenberg[3], Sven Petersen[2]

[1] Department of Maritime Technologies, BAUER Maschinen GmbH, BAUER-Str. 1, 86529 Schrobenhausen, Germany,

Present affiliation: BASF Construction Solutions GmbH, Dr.-Albert-Frank-Straße 32, 83308 Trostberg, Germany, giovanni.spagnoli@basf.com

[2] GEOMAR - Helmholtz Centre for Ocean Research Kiel, Wischhofstraße 1-3, 24148 Kiel, Germany

[3] GFZ German Research Centre for Geosciences, Geothermal Energy Systems, Telegrafenberg E253, 14473 Potsdam, Germany

Abstract

Deep-sea mining exploration for seafloor massive sulfide (SMS) deposits is currently increasing. At present, most exploration activities are surficial and use indirect methods to identify potential sites and perform first assessments. For a proper resource estimate, however, drilling is inevitable. By using seabed drill rigs, exploration costs can be reduced considerably. SMS deposits are normally found at depths between 1,000 - 4,000 m and in order for deep sea mining to be implemented, reliable technologies are needed. Additionally, the development of geophysical systems that can detect and classify mineralized zones from waste materials while drilling could decrease costs and speed up offshore operations by limiting the amount of drilling of unmineralized materials. This paper shows how the physical properties of SMS can be used to discriminate between host rocks and mineralization. Seismic P-wave velocities (Vp) were measured on 40 SMS and unmineralized mini-cores. By back-calculating the porosity from Vp, comparing the results with electrical resistivity measurements, and using Archie's Law, it is possible to observe that metallic conduction exists. For deep-sea mineral exploration, the combination of seismic tests, electrical resistivity and magnetic susceptibility could support the preliminary discrimination of mineralized samples in the cores while drilling at the seafloor.

Key words: seafloor massive sulfides; deep-sea mining; P-wave measurement; mineralization; petrophysical properties.

1. Introduction

The increasing demand for metallic raw materials is becoming an important opportunity for deep sea mining, which serves to relieve the land-based metal mining industry. Due to the recent increasing demands through the industrialization of countries such as China and India, seafloor massive sulfide (SMS) mining is presently being investigated (Birney et al., 2006; Boschen et al., 2013). Since 2011 six contracts for the exploration of seafloor massive sulfides have been approved by the International Seabed Authority in areas beyond national jurisdiction (France and Russia in the Atlantic Ocean; China, Korea, India and Germany in the Indian Ocean) and Japan, Korea and France have developed strong national programs within their Exclusive Economic Zones in the Pacific (Petersen et al., 2016).

Current deep-sea mining technologies are based on mining technologies commonly used on land, such as surface mining (see Cardu and Mucci, 2013). For instance, Nautilus Minerals Inc. is developing a deep-sea mining system for SMS deposits in Papua New Guinea using three different machines, i.e. the Auxiliary Cutter (AC), the Bulk Cutter (BC) and the Collecting Machine (CM). Other technologies are more focused on novel mining approaches (Birney et al., 2006; Spagnoli et al., 2016a).

Seafloor hydrothermal venting in the geological past produced some of the largest and most valuable ore deposits mined to date such as those in the Iberian Pyrite Belt and the Urals, where individual deposits can reach hundreds of millions of tons (Hannington et al., 2005). SMS deposits are currently forming in the deep oceans at tectonically active spreading systems (mid-oceans ridges and "back-arc" spreading centers) where hydrothermal vents expel sulfide-rich mineralizing fluids into the ocean in water depths up to 4000 m (Hannington et al., 2005). These systems are the result of global heat dissipation from the mantle to oceanic crust. The circulating and heated solutions (> 400° C) are mixed with cold seawater and form the most striking appearance of submarine SMS, several meter-high chimneys. These structures eventually erode and decay, forming mounds that can reach several hundred meters in diameter. Larger sulfide deposits are the product of several hydrothermal generation cycles.

Massive sulfides are polymetallic in character by having valuable trace metals in addition to the economically most important metals copper (Cu) and zinc (Zn). These trace metals include silver (Ag), gold (Au), antimony (Sb), cadmium (Cd), gallium (Ga), germanium (Ge), and indium (In) (Monecke et al.,

2016). According to Singer (1995), volcanic-associated and sedimentary-exhalative massive sulfide deposits have accounted for more than half of the past global production of Zn and Pb and a significant amount of Au and other byproduct metals. The metal inventory at the seafloor could be huge, however, resource estimates for the deep-sea fall into the "indicated resources" category at most. Nevertheless, ongoing exploration work of some license holders such as COMRA, Ifremer, BGR, to name a few (Petersen et al., 2016), is constantly producing new discoveries. The assessment of these discoveries by sampling and drilling is important in order to determine if ocean-floor mineral tenements host sufficient grade and size to justify a future potential mining operation (Birney et al., 2006). Geotechnical (Spagnoli et al, 2016b), mineralogical (Hannington et al., 2011), and geophysical (Swidinsky et al., 2012) assessments of SMS deposits can subsequently be used to ground-truth large-scale geophysical surveys.

Spagnoli et al. (2016c; 2017) previously investigated the electrical and magnetic susceptibility properties on 40 mini-cores chosen to be a representative suite of rock and ore types from various SMS deposits. It was shown that it is possible to discriminate the mineralization from the host rock based on these physical rock parameters. P-wave velocity measurements (Vp) performed in the laboratory are quite common in rock mechanics studies (e.g. Castagna et al., 1985; Chang et al., 2006; Elbra et al., 2011; Brotons et al., 2014; Saito et al., 2016). They have been performed on massive sulfide deposits on land, e.g. Salisbury et al. (2000); Morgan (2012); Bellefleur et al. (2012); Malehmir et al. (2012; 2013), Miah et al. (2015). Miah et al. (2015) showed that hydrothermal alteration considerably increases Vp and density of altered argillite and felsic volcanic rocks in comparison to their corresponding unaltered facies. Malehmir et al. (2014) showed that the host rock velocities increase from felsic to ultramafic rocks, with Vp velocity of 7.5km/sec for the Kevitsa main intrusion (mafic–ultramafic Ni–Cu–PGE deposit) and 6.5km/sec and 5.7km/sec for the Ventersdorp Supergroup lava and Central Rand Group quartzite respectively.

Compared to massive sulfide deposits on land, few data are available for marine SMS samples. Ludwig et al. (1998) investigated the physical properties and ultrasonic velocity on 24 mini-cores recovered at the Trans-Atlantic Geotraverse (TAG) hydrothermal mound during Ocean Drilling Program Leg 158 at confining pressures up to 100 MPa. They found that a general increase in Vp with depth is observed for all samples and is probably caused by increased cementation and silicification of the mostly

brecciated rocks. Rocks of Zones 2 (anhydrite-rich) and 3 (silicified wallrock breccias) show a seismic velocity dependence on total sulfide mineral concentration. With increasing anhydrite concentration, Vp decreases linearly. Vp ranges between 3 and 6 km/s for 5 MPa confining pressure.

Yamazaki et al. (1990) investigated the Vp on six SMS core samples of 60 x 30 mm. The results showed that Vp ranged between 2.5 and 3.5 km/s. Yamazaki and Park (2003) performed geotechnical tests and also Vp measurements on eight SMS cores the Izena Cauldron at Okinawa Trough. No clear correlation between mineralogy and Vp was drawn, whereas the results showed a trend where the Vp was inversely proportional to the porosity. Assessment of porosity will therefore be key information in determining the mineralization content of a SMS core. Yet, porosity is difficult to be assessed *in situ* during drilling operations. In this context, Vp measurements could be used to indirectly assess it and combine this with other geophysical measurements. The purpose of this study is to measure the seismic/acoustic P-wave velocity of a representative set of mini-cores of different types of SMS and their host rocks for comparison with previous physical property measurements, i.e. electrical and magnetic susceptibility properties. A variety of sample types from different volcanic and tectonic settings represent a range of physical properties found in the ore material (different grain size and bounds of sulfide minerals; variable mineralogy and porosity) and the host rock (different rock types, altered, unaltered). The results of this study suggest that a comparison of P-wave velocity with other physical properties (e.g., porosity, bulk density, magnetic susceptibility, resistivity) could help the development of software packages that may detect SMS mineralization and altered host rocks while drilling-and-recovering cores in deep-waters with seabed drill rigs. This could decrease costs and speed up offshore mineral exploration with underwater drill rigs by limiting the amount of drilling in unmineralized material (Spagnoli et al., 2016c).

2. Material and methods

During sample selection care has been taken into account to identify samples representing different mineralogical types of seafloor massive sulfides from a variety different tectonic settings. The mineralogy of the sulfides depends on the physico-chemical conditions during formation, which reflect variable host rock compositions (related to the tectonic setting), water depth, formation temperature, permeability below the seafloor, and magmatic activity (Hannington et al., 2005). The mineralogy of seafloor sulfides is,

however, quite simple and the samples described by Spagnoli et al. (2016c), were taken due to their Fe-, Cu-, and Zn-rich enrichment, e.g. typical samples with very high grades of the respective major metals and minerals, e.g. chalcopyrite (Cu), sphalerite (Zn), and pyrite (Fe). Because the tectonic setting has a profound impact on the mineralogy and geochemistry of the SMS occurrences, specimens were chosen from a back-arc basin site (Pacmanus), from slow-spreading (basalt-hosted: Turtle Pits; ultramafic-hosted: Logatchev and Irinovskoe), intermediate-spreading ridges (Galapagos and Axial Seamount), and fast-spreading mid-ocean ridges (EPR South and Pacific-Antarctic Ridge) (Fig. 1).

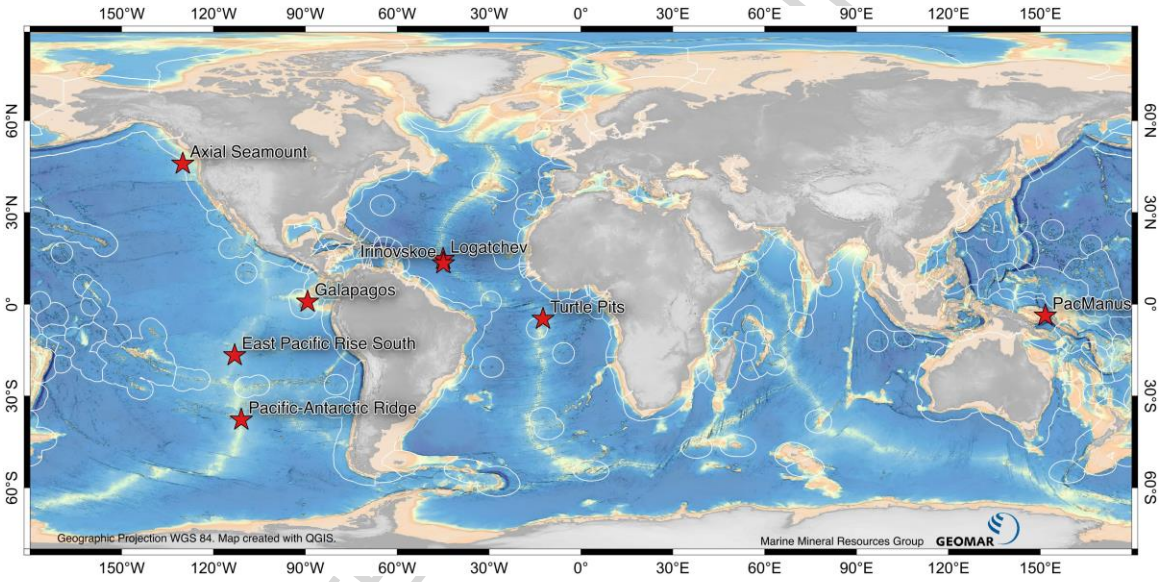

Fig. 1. Location of the sample used for the laboratory experiments.

2.1 Sample description

A set of 40 mini-cores was extracted from a variety of oceanic rocks including; chimneys, massive sulfides, and host rock. Each mini-core was drilled from a parent sample using a Karl Dahm drill press fitted with a standard 1 inch-diameter diamond-impregnated drill bit. The samples have a diameter of 25.4 mm, and a length between 17.55 mm and 45.88 mm (average 37.14 mm). The samples were cut at the International Ocean Discovery Program's (IODP) Bremen Core Repository (BCR) in Bremen, Germany. A combination of two rocks saws (Fig. 2) were used including an ASC Scientific Dual Blade Rock Saw and an IODP single blade rock saw. All of the samples were cut using tap water to cool and clean the diamond saw blade. For the ultrasonic measurements, precise cuts resulting in parallel end faces are neces-

sary to reduce measurement error during the velocity experiments. Due to the high-quality parallel end faces, the error in length determination is about ± 0.05 mm.

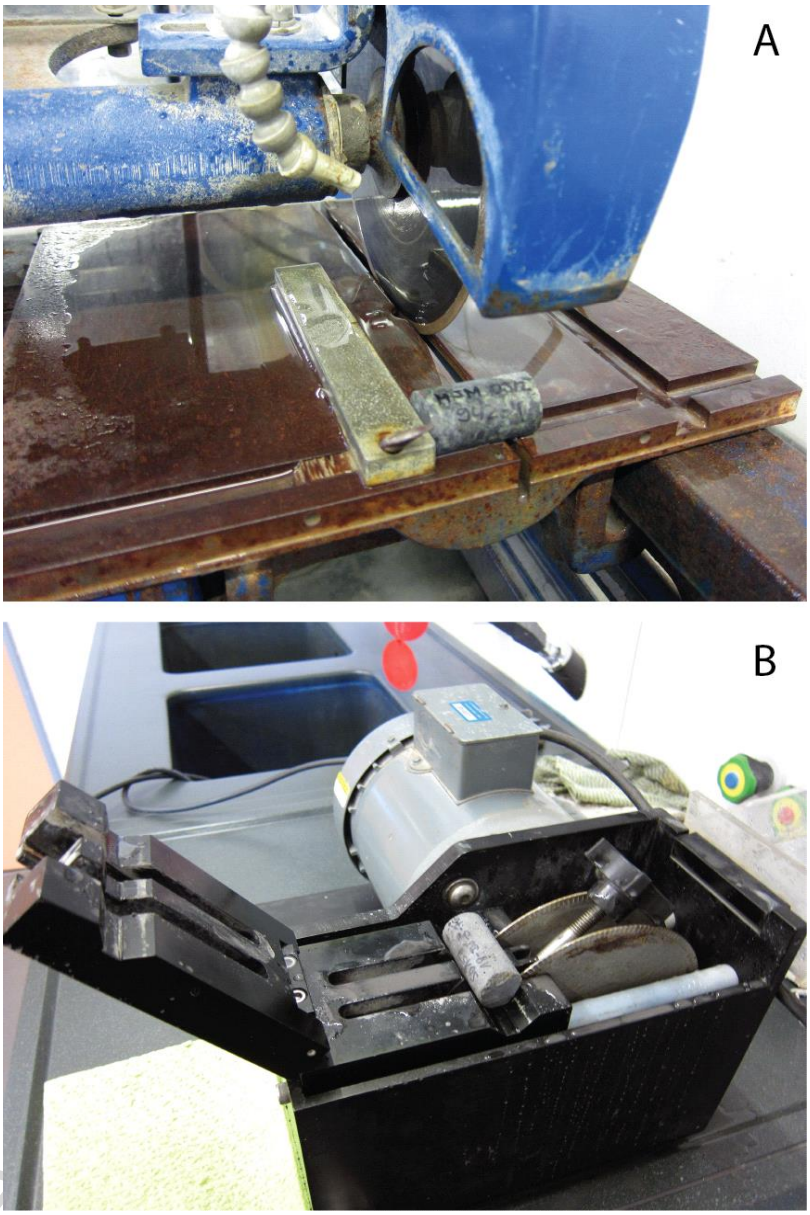

Fig. 2. Rock saws used at the BCR for making precise and parallel cuts. A) standard IODP single 10-inch blade rock saw, and B) ASC Scientific Dual Blade rock saw.

2.2 Ultrasonic P-wave measurements

The experiments were performed at the petrophysical laboratory of the German Research Centre for Geosciences (GFZ) in Potsdam, Germany. The system used for the measurements consists of an ultrasonic pulser (Panametrics Model 5058PR), a digital oscilloscope (Agilent DSO 6012A), a sample holder (Geotron UMV 420) and two transducers (Panametrics V 103-RM) (Fig. 3). The pulser provides a high voltage pulse to fire the ultrasonic transmitter. The pulse voltage is switchable between 100 V, 200 V, 400 V and 900 V (11 µJ, 44 µJ, 176 µJ – 891 µJ). The pulse repetition rate is variable in different steps between, 20 Hz and 2 kHz. For this study, we used a constant rate of 1 kHz. A TTL compatible trigger signal is provided with the pulse to drive the oscilloscope. Furthermore, the pulser contains a signal conditioning unit to improve the quality of the received signal by filtering and amplification. The signal output is connected to the digital storage oscilloscope. The oscilloscope with a bandwidth of, 200 MHz (2 GSa/s) allows to average the signal for further signal quality improvement and to store the signal digitally.

We determined the P-wave arrival using the cursor function of the oscilloscope on a stacked signal (average over 128 wave forms to improve signal to noise ratio). To make sure that the coupling between sample and transducers will not influence the measurements, a coupling fluid was used between the sample and transducers, which are pushed on the sample surface with a constant pressure of one bar using the pneumatic contact pressure piston system of the sample holder (Fig. 3). To correct the system related time shift due to a possible difference between the high voltage pulse and the start of the oscilloscope, the transducer characteristics, coupling influences etc., we measured a travel time curve with three aluminum reference cylinders (30 mm, 50 mm, and 100 mm length). The slope of the curve gave us the reciprocal velocity of the aluminum (1/(6400m/s)) and the intercept with the time axis provides the time shift (270 ns), which then has to be subtracted from the measured P-wave arrivals. The velocity was calculated by the following equation:

$$v = l/(t_t - t_s) \quad (1)$$

where, l is the sample length in mm, t_t is the measured travel time in µs, and t_s is the time shift.

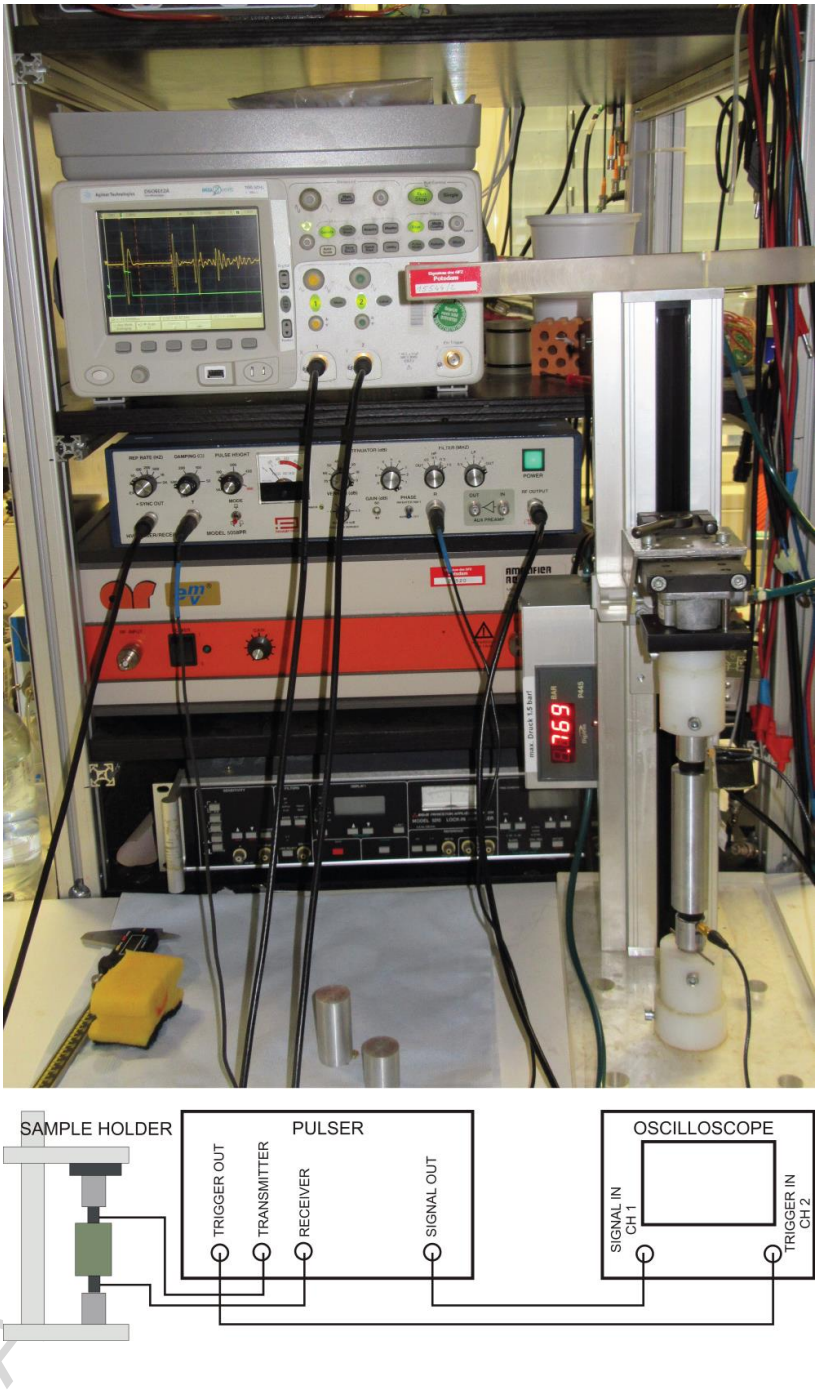

Fig. 3. Principle setup for the ultrasonic P-wave velocity measurements.

2.3 Velocity measurements

Velocity measurements were carried out on both the dry and fully water-saturated samples. Tap water was used as a fluid, as the focus was to observe the differences between the sample groups in absolute values. Experiments were performed twice on both dry and wet samples to check measurement

repeatability. The difference between the first and second measurements was up to 5%, which we assumed negligible. Air drying of the samples was carried out in a vacuum oven at 105 °C and about, 20 mbar for 12 hours. After the dry measurements were performed, samples were evacuated in an exicator to about 5 mbar (water vapor pressure at, 20 °C is about 23 mbar). Degassed tap water was injected until the samples were completely covered with water. Atmospheric pressure was applied to the water covered samples for 12 hours before the measurements were taken. The measured velocities vary between 6300 m/s and 2700 m/s. With a central frequency of the transducers of about 1 MHz, the wavelengths are on the order of 3 mm to 6 mm. Some of the samples have pores and vugs with dimensions on the order of the wavelength and even bigger, which resulted in a strong scattering of wave energy. For some of the samples the attenuation due to scattering was so strong, that no or just a very weak signal reached the receiver. Thus, we were not able to get evaluable signals and hence velocity data for all of the dry samples, particularly for dry copper-rich cores but also for one Zn and one host rock sample. Fig. 4 shows examples for a strong first arrival (A) and the situation where a very weak signal for the saturated sample and no signal for the dry sample could be detected (B) at maximum signal amplification (see cutoff of the electrical crosstalk signal of the high voltage transmitter pulse). A good quality first arrival can be picked with an accuracy of about ± 0.01 µs and better. For an attenuated weak first arrival, the error increases to ± 0.2 µs. Together with the error in length of about ± 0.05 mm, this results in an accuracy for the velocity of about 0.2% for strong signals and about 4% for weak signals. To indicate the number of samples where no signal could be detected (see Fig. 4 B, dry signal), they were plotted with zero velocity in the following graphs.

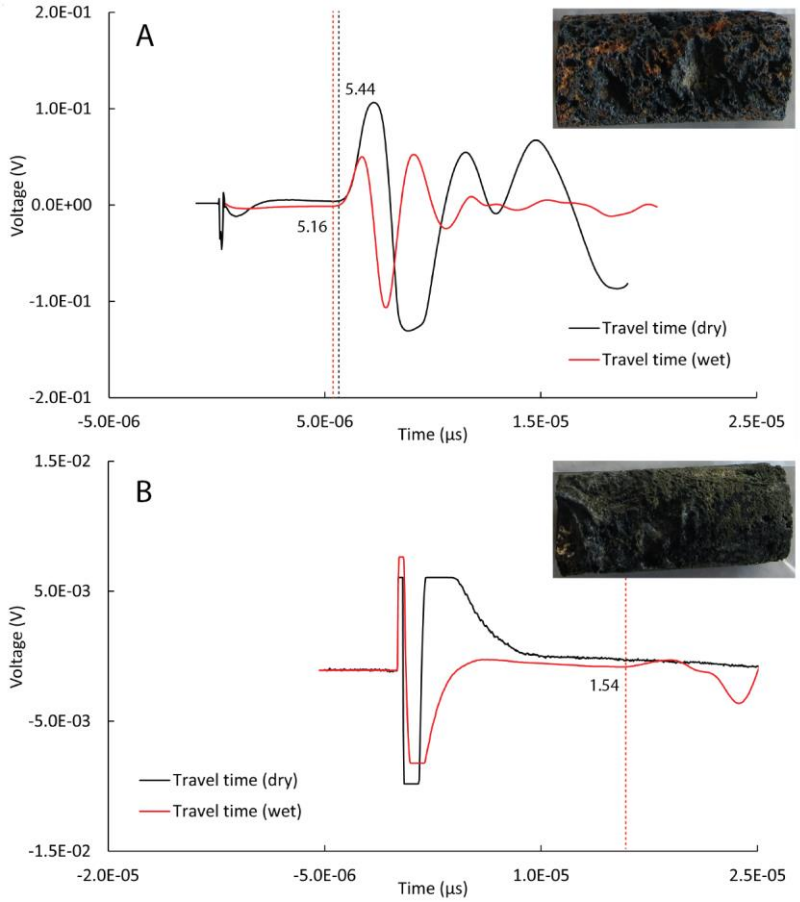

Fig. 4. Examples of first arrivals used to calculate the velocities for the dry and wet ultrasonic measurements. A) Sample S0166 59 GTVA-1B1 (chimney Zn-Ba) showing a strong signal for both dry (5.44 µs) and wet (5.16 µs) first arrivals. B) Sample S0208 DR100-3A (chimney Zn) showing no signal for the dry measurement, and a weak signal for the wet (1.54 µs) first arrival. The cutoff of the crosstalk signal from the high voltage transmitter pulse illustrates the high amplification of the record.

2.4 Electrical resistivity and magnetic susceptibility

Vp results have been compared with previous experiments (Spagnoli et al., 2016c; 2017). Electrical resistivity and magnetic susceptibility are briefly described. In order to determine the frequency-dependent complex electrical resistivity in the frequency range between 0.002 Hz and 100 Hz, cylindrical samples of 50mm length and 25mm diameter were tested (see Spagnoli et al., 2016C for the details). A 4-point electrode configuration was used. The samples were saturated with a NaCl solutions with conductivity of 5S/m (see Spagnoli et al., 2016c for the details).

Regarding the magnetic susceptibility tests (see Spagnoli et al., 2017 for the details), the same cylinders as for the electrical resistivity measurements were used. A Minikappa KLF-3 Magnetic Susceptibility Meter from AGICO was used. The pick-up unit comprised a vertically aligned coil which generated a homogenous sinusoidal magnetic field at the sample position with an amplitude of 50A/m and a frequency of 2kHz. The core was placed in the sample holder and each sample was measured three times.

3. Results and discussion

Table 1 shows the results obtained from repeat Vp measurements for both dry and wet conditions. Porosity, bulk density, wet (Spagnoli et al., 2016c) and dry electrical resistivity (Hördt et al., 2016), together with magnetic susceptibility values (Spagnoli et al., 2017) are also included and are later used for the comparison plots with the Vp data. Figs. 5 and 6 show the results of Vp compared with the porosity, and bulk density, respectively. Porosity and density were calculated from the weight of the dry and saturated samples, the buoyancy weight and the density of the fluid (Spagnoli et al., 2016c).

Fig. 5 (Vp vs. porosity) shows a strong decrease of Vp values with increasing porosity for dry conditions, the same is true also for wet conditions. The scattering of the data is attributed to the fact that the “porosity value” does not distinguish between different pore types occurring in the samples (intergranular pores, cracks, solution pores, etc.), which have a different influence on velocity. Furthermore, the dependence of velocity on porosity is superimposed by differences in mineralogical composition and mineralization content. P-wave velocity values for basalt in saturated conditions range between 4.5 and 6.8 km/s, which agree with the values provided Bourbié et al. (1987) and Ludwig et al. (1998). The effect of a general decrease in P-wave velocity with increasing porosity is due to the increase in porosity reducing the elastic moduli of the rock skeleton that decreases Vp (e.g. Miller and Stewart, 1990; Kassab and Weller, 2015). Mineralized samples have larger porosities and larger bulk densities if compared with the non-mineralized specimens. It is well-known that SMS samples have larger porosities than samples obtained from massive sulfide deposits on land due to compaction of the mineralization during ageing and tectonic uplift (e.g. Tufar, 1991; Gröschel-Becker et al., 1994; Tivey et al., 1998; Zhu et al., 2007).

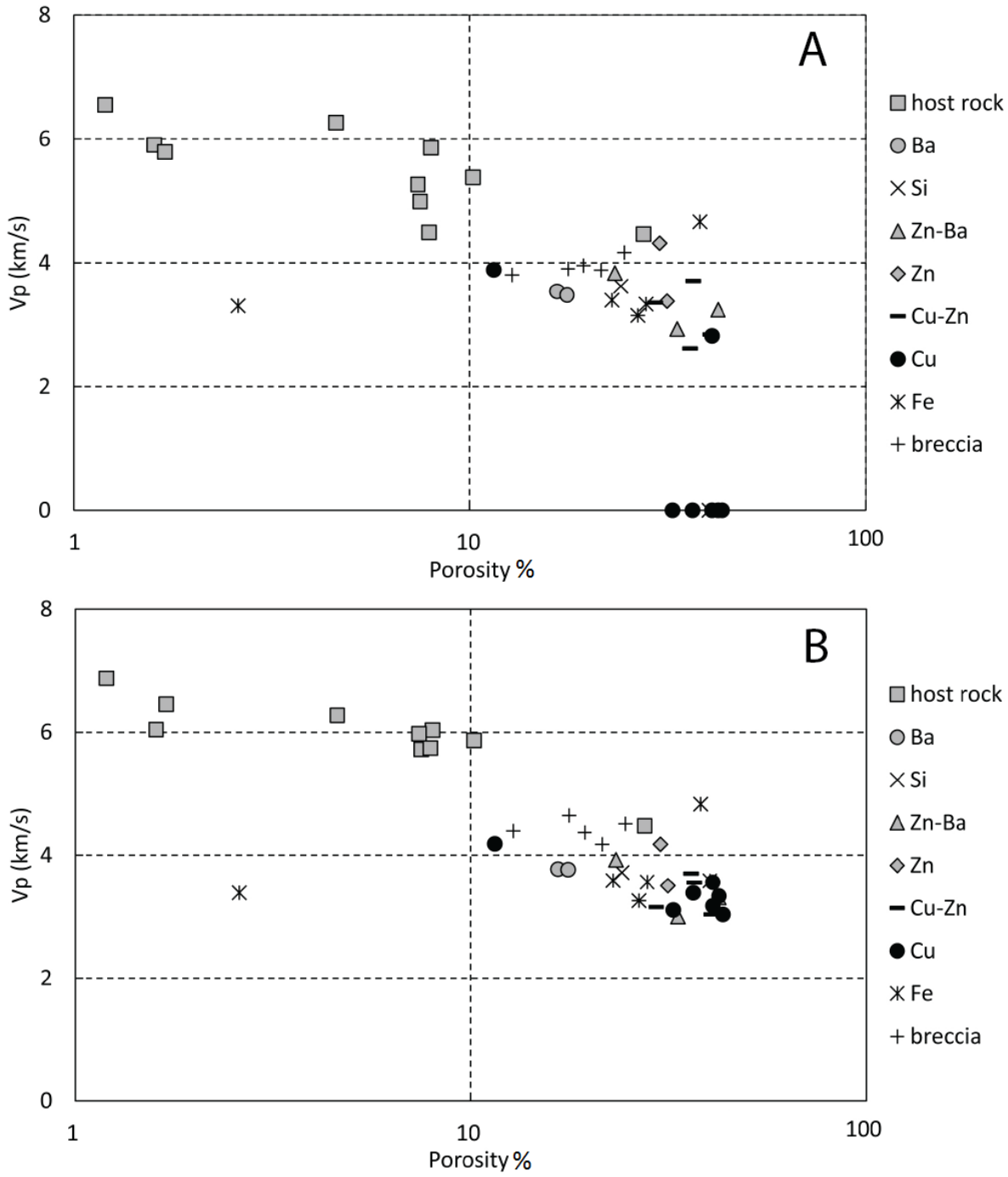

Fig. 5. Comparison plots of dry (A), and wet (B) velocity measurements vs. porosity. Note: data points that lie on the x-axis in (A) represent samples with no signal and distinguishable first arrivals.

The Vp values (for dry and wet conditions) range between 3 and 6 km/s. The results are slightly higher when compared to values reported by Yamazaki et al. (1990) and Yamazaki and Park (2003), who performed tests under atmospheric conditions, as well. Ludwig et al. (1998) performed Vp and Vs tests for simulating deep (rock) conditions with confining pressures ranging from 5 to 100 MPa. They show that by increasing the confining pressure, Vp values increase up to 10-15%, probably related to pressure induced porosity reduction, improvement of grain to grain contacts, and closure of micro cracks. Based on absolute velocity values, the host rock and breccia exhibit higher velocities (> 4.2 km/s) than mineralized cores, at least at atmospheric pressure. From Fig.5 it appears that the host rock samples show a stronger dependence on porosity than the mineralized samples, which is probably due to the fact that this porosity dependency is not superimposed by the influence of sulfide content on velocity.

In general, velocity increases with increasing density because the denser minerals show higher elastic moduli. For a given mineralogical endmember composition, density and velocity increase with decreasing porosity. Fig. 6 shows the velocities values against the density values. If the velocity would be primarily influenced by the mineral composition, we would expect to see a positive correlation between velocity and density, because the denser minerals show higher elastic moduli. However, we observe that the high-density samples have a low velocity. We attribute this to the fact that the high-density samples with high ore contents are at the same time the most porous samples. The higher density of mineralized samples is mainly due to the higher specific density of Cu-, Zn-, and Fe- containing sulfide minerals.

The high porosity is related to the formation of the mineralized samples in chimneys above the seafloor. During precipitation of the sulfides abundant pore space is formed and therefore the mineralized samples have a higher porosity when compared to the low-porosity host rocks. A similar lack of expected correlation has been observed for land data (Bellefleur et al., 2012) for VMS samples from two different regions. The authors attributed the change in velocity to a variability in grain sizes and pyrite content. In principle difference in grain sizes/ore content could also be a possible explanation for our data. Yet, give that our samples are biased towards high porous samples since they have been collected by in the chimney areas and not at depths from the stockwork, we argue that for this sample set porosity seems to be the more important factor determining the velocity. However, for low porous samples at depth, velocity changes may yet well be related to grain size variations as for the VMS samples.

Considering Fig. 6B (Vp vs. bulk density in wet conditions), it is possible to see that host rock samples “host” and “mineralization” separate at a Vp value of about 4.2 km/s, with the exception of one sample.

From Fig. 6 it appears that the host rock samples show a stronger dependence on porosity than the mineralized samples, which is probably due to the fact that this porosity dependency is not superimposed by the influence of sulfide content on velocity.

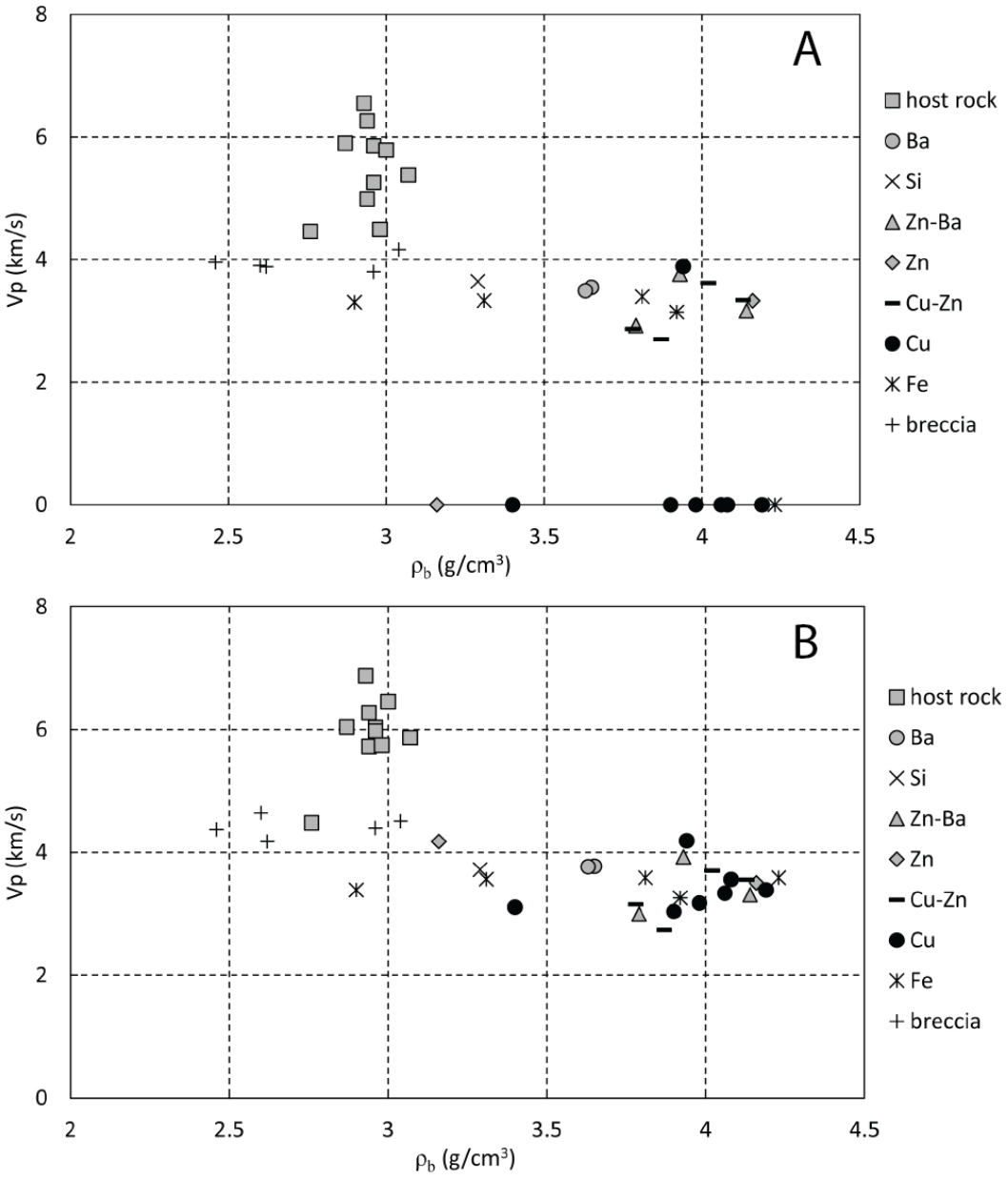

Fig. 6. Comparison plots of dry (A), and wet (B) velocity measurements vs. bulk density. Note: data points that lie on the x-axis in (A) represent samples with no signal and distinguishable first arrivals.

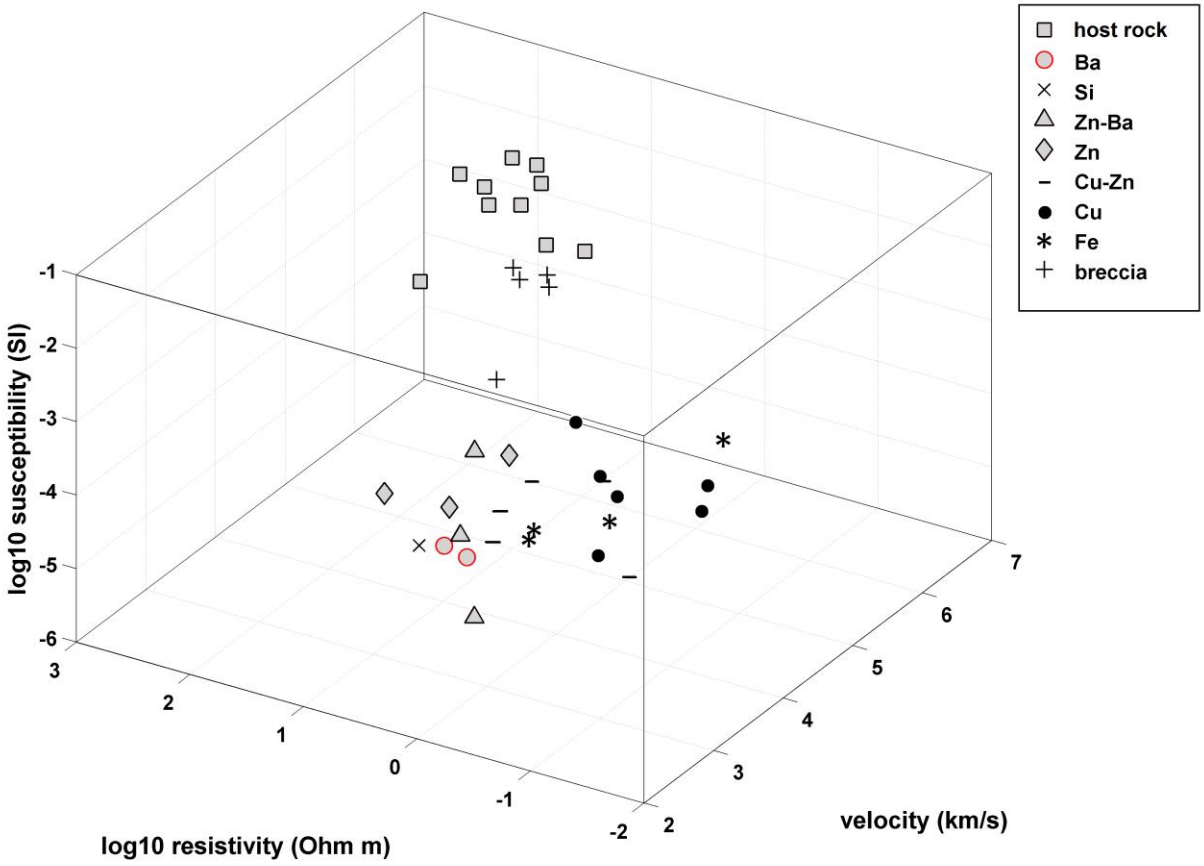

Fig. 7: 3D plot of velocity, resistivity and magnetic susceptibility (the latter are from Spagnoli et al., 2016c and 2017). In comparison to basalt host rock, mineralized cores exhibit lower resistivity, higher velocities and higher susceptibilities. The red color for the Ba samples means negative SI values.

Spagnoli et al. (2016c, 2017) observed that the electrical resistivity, ρ, is a function of porosity, Φ, and mineral content, whereas the magnetic susceptibility, χ, is only a function of mineralization, i.e. the presence or absence of mineralized samples. Fig. 7 shows a 3D plot of wet velocity, magnetic susceptibility and electrical conductivity. In terms of distinguishing whether cores are mineralized or not, low values of magnetic susceptibility seem to be the clearest indicator of whether cores have undergone hydrothermal circulation and are mineralized. Also, magnetic susceptibility is not dependent on other parameters,

i.e. porosity, such that they can be regarded as a direct indicator. Low resistivity may also be an indicator, since the electrical resistivity of mineralized samples is few orders of magnitude smaller than the host basalt. For electrical resistivity, the dependence on porosity still needs to be considered, though. Most of the resistivity variations observed fall in a range which may be explained by Archie's Law, i.e. can be attributed to a large extent by electrolytic conduction within the pore fluid of these highly porous samples. If the pore fluid is the only conducting phase in the rock, the rock conductivity is well described by Archie's equation. If there are other conductivity contributions from the solid rock components (conducting/semiconducting minerals) or the fluid-solid-interfaces (surface conductivity) the rock conductivity can be expressed as follows (e.g. Worthington, 1985):

$$\sigma_b = \sigma_{el} + \sigma_a \text{ with: } \sigma_{el} = \frac{\sigma_w \Phi^m}{a} \quad (2)$$

where, σ_b denotes the rock conductivity, σ_a the additional conductivity contributions from conducting/semiconducting minerals and surface conductivity, and σ_{el} the electrolytic conductivity contribution of the pore fluid described by the Archie-equation (σ_w -conductivity of the pore fluid, Φ – porosity, a – tortuosity factor). For highly mineralized samples and in situations where the semiconducting/conducting mineral phases form a continuous connected network throughout the rock, the additional conductivity contribution can be very large compared to the electrolytic conductivity contribution ($\sigma_a \gg \sigma_{el}$).

For copper and iron rich samples, however, this is not the case. Here, electrical resistivity values are too small to be explained by pore fluid conduction. For these cores the measured low resistivities can only be explained by the content of semiconducting/conducting mineralization (see Spagnoli et al., 2016c).

During drilling campaigns, well logging easily provides ρ, Vp, and χ data. Porosity measurements *in situ* on the other hand are difficult and expensive, and therefore they are normally derived in the laboratory, for instance using a permeameter (Zhu et al., 2007). However, given that Vp is mainly function of the porosity, Φ, it should be possible to determine Φ from Vp and use this information to constrain resistivity measurements in order to preliminary assess the presence of mineralization in the cores. Due to the fact that all physical properties are available on our cores, it is possible to test this hypothesis. Fig. 8 shows the calculated porosity from the wet velocity vs. the measured porosity values. A clear correlation, with a coefficient of determination (R^2), of 0.62, is visible between predicted and experimentally measured porosity.

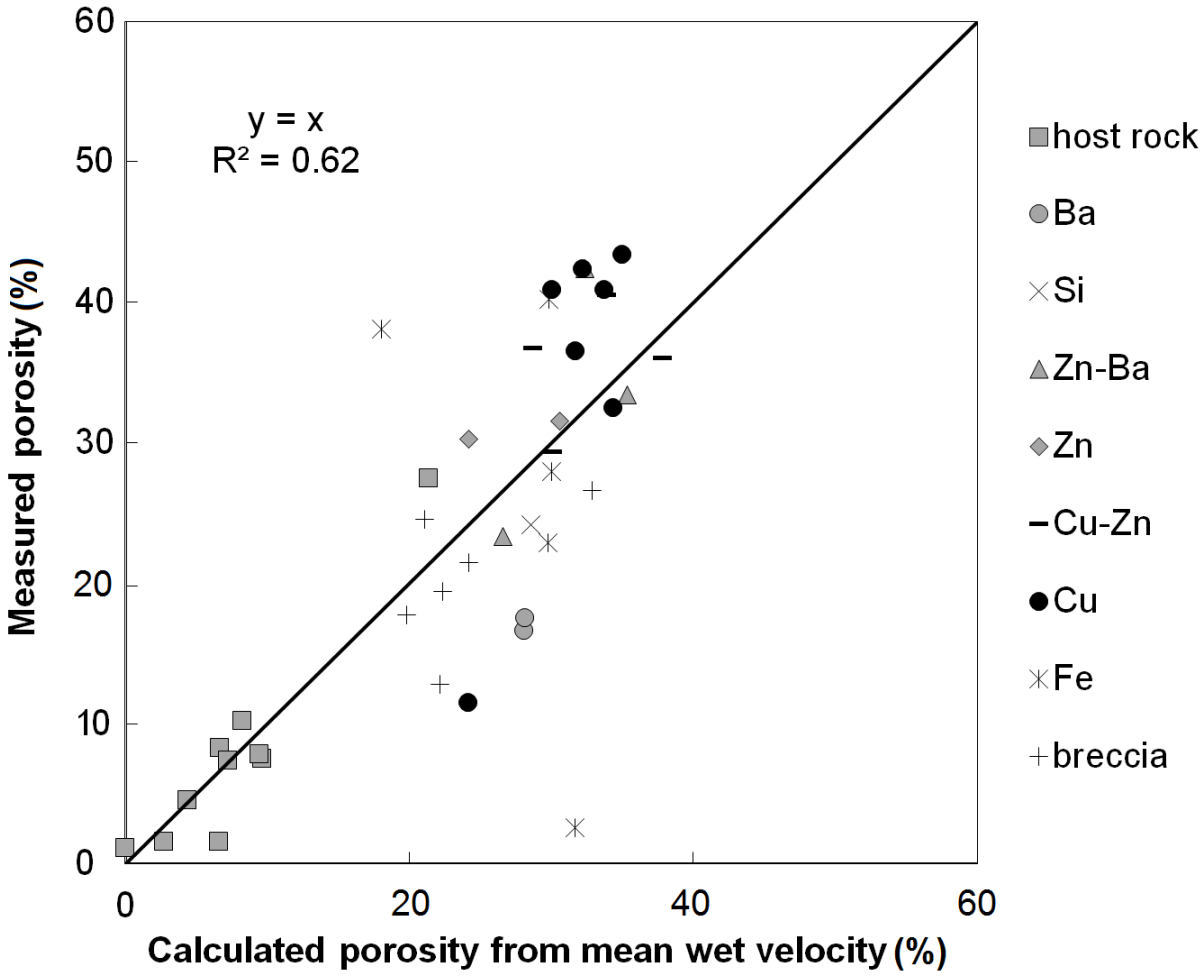

Fig. 8. Comparison between calculated porosity from Vp measurements on wet samples and measured porosity.

Fig. 9A shows the measured electrical resistivity as a function of measured porosity. Overlain on the plot is the expected resistivity calculated with Archie's equation with different empirical parameters *a* and *m*. During the electrical experiments performed on saturated SMS samples, highly conductive NaCl solution with 5S/m conductivity was used to saturate the samples to simulate the seafloor conditions. Regarding the tortuosity factor, *a*, we assumed a value of 1, whereas for the cementation factor, *m*, we assumed a value of 1.3 for unconsolidated sediments, and 2.4 for more consolidated rock (Schön, 2004).

The measured electrical resistivity values will be used as a benchmark to which we compare calculated resistivities based on porosity derived from velocity measurements. These are shown in Fig. 9B for the electrical resistivity predicted by porosity derived from Vp dry and Fig. 9C for porosity derived Vp wet. The data show an acceptable match with the measured data versus the calculated ones, particularly with the wet conditions. For the predicted porosity/resistivity values, SMS specimens containing Cu-Zn, Fe, Zn and Cu are below the Archie curve with a = 1 and m = 2.4. Archie's equation describes the resistivity of a porous rock, assuming that the brine in the pore space is the only conducting phase. As mentioned above, the semiconducting/conducting ore minerals provide an additional conductivity contribution, which is not considered in Archie's equation. For instance, Chalcopyrite ($CuFeS_2$) and Pyrite (FeS_2) may show resistivities in the order of 10^{-4} Ωm and even less (e.g. Schön, 2004; Pridmore and Shuey, 1976; Pearce et al., 2006). Compared to the resistivity of 0.2 Ωm for the used brine, the conductivity contribution from the ore minerals can easily be orders of magnitude higher than the electrolytical conductivity contribution and explains why the measured values fall below the Archie-curves. This could indirectly be derived from the Vp values during drilling and recovery campaigns.

Table 1. List of samples investigated in this study, with rock type, dominant mineralogy, density, electrical resistivity, magnetic susceptibility, and results of the repeat ultrasonic velocity measurements. Porosity values are given as volume fraction according to the definition of V_{pore}/V_{probe}.

No.	Sample name	Material	Length (mm)	Bulk porosity	Bulk density (g/cm^3)	Electrical resistivity (Ωm) wet	Electrical resistivity (Ωm) dry	Magnetic susceptibility (SI)	1st Dry velocity (km/s)	2nd Dry velocity (km/s)	1st Wet velocity (km/s)	2nd wet velocity (km/s)
1	MSM03/2-928DR-5	Host rock	38.41	0.08	2.96	124.4	12139.94	0.00764	5.54	5.77	5.73	5.99
2	MSM03/2-929DR-2	Host rock	39.64	0.016	2.87	70.27	16263.34	0.00366	6.04	6.18	6.10	6.34
3	MSM03/2-942DR-1	Host rock	37.81	0.017	3	17.79	5181.228	0.0008	5.69	5.89	6.32	6.59
4	MSM03/2-942DR-4	Host rock	39.7	0.012	2.93	85.91	8249.907	0.00299	------	6.55	6.79	6.97
5	MSM03/2 943DR-10	Host rock	37.83	0.075	2.94	48.79	1145.813	0.0129	4.99	4.99	5.69	5.75
6	S0109/3-69GTVA-3b	Host rock	30.43	0.046	2.94	60.4	51663.36	0.0118	6.16	6.37	6.12	6.42
7	S0157-15DS-1 FG	Host rock	40.96	0.275	2.76	31.06	833.6704	0.0063	4.46	4.46	4.41	4.54
8	S0157-17DS-4 FG	Host rock	38.15	0.079	2.98	23.87	1612.609	0.0097	4.52	4.47	5.61	5.87
9	S0157 18-DS-5-FG	Host rock	41.6	0.102	3.07	18.92	21988.54	0.0171	5.24	5.52	5.77	5.96
10	S0157 38 DS-Tubaf	Host rock	37.88	0.074	2.96	19.81	2138.76	0.00204	5.22	5.31	5.86	6.09
11	S0109/2-89GTV-M	Ba	41.54	0.166	3.65	4.42	23366.13	-8.3E-06	3.55	3.53	3.68	3.87
12	S0109/2-89GTV-M 2nd	Ba	37.57	0.176	3.63	6.96	106596.2	-9.9E-06	3.49	3.46	3.67	3.86
13	EPR-South	Si	47.65	0.241	3.29	10.82	9317.477	-8.9E-06	3.65	3.59	3.65	3.79
14	S0166-59GTVA-1B1	Zn-Ba	17.16	0.424	4.14	1.99	235403.4	3.86E-06	3.17	3.31	3.12	3.50
15	S0166-	Zn-	45.85	0.334	3.79	1.7	2927.96	0.00009	2.92	2.94	------	3.00

	70GTVA-1C4	Ba										
16	S0166-70GTVA-1G1	Zn-Ba	44.78	0.233	3.93	4.68	1358.332	0.000177	3.77	3.91	3.86	3.99
17	S0166 58GTVA-8A1	Zn	45.57	0.315	4.16	16.13	26806.22	5.41E-05	3.33	3.43	3.46	3.54
18	S0208-DR100-2A	Zn	44.8	0.302	3.16	3.31	20.5741	0.000118	------	4.32	4.07	4.28
19	S0109/2-81GTVA-2(1)	Cu-Zn	40.47	0.36	3.87	0.49	70.6264	0.000109	2.70	2.53	2.72	2.75
20	S0109/2-81GTVA-2(2)	Cu-Zn	42.94	0.367	4.02	0.28	10.2047	0.000557	3.62	3.80	3.60	3.80
21	S0166-59GTVA-2A1	Cu-Zn	37.94	0.294	4.13	1.8	676.6364	0.000453	3.34	3.37	3.66	3.44
22	S0166-58GTVA-6A	Cu-Zn	29.95	0.405	3.78	0.07	2.7738	2.77E-05	2.87	2.81	------	3.15
23	S0208-DR100-3A	Zn	45.96	0.434	3.9	0.11	0.27061	8.62E-05	------	------	------	3.04
24	ODM-ROC-V557-324	Zn	26.45	0.115	3.94	0.06	2.0379	0.000247	3.89	------	3.84	4.53
25	ODM ROC-V557-327	Cu	39.87	0.325	3.4	0	0.024111	0.000154	------	------	------	3.11
26	M64/1-114ROV-4E(1)	Cu	34.81	0.424	4.06	0.02	1.272985	0.000264	------	------	------	3.34
27	M64/1-114ROV-4E(2)	Cu	32.5	0.409	3.98	0.09	0.36045	0.00018	------	2.82	------	3.17
28	S0109/2-81GTV-4(1)	Cu	42.83	0.409	4.08	0.36	1.3756	0.000756	------	------	------	3.56
29	S0109/2-81GTV-4(2)	Cu	37.17	0.365	4.19	0.17	0.41106	0.000803	------	------	3.25	3.53
30	M64/1-124GTV-2E	Fe	42.78	0.402	4.23	0.19	0.92144	0.00234	------	------	------	3.58

31	M64/1-124-GTV-2I	Fe	41.43	0.381	4.61	0.11	0.22746	0.000908	4.58	4.74	4.69	4.97
32	M78/2-297ROV-1C	Fe	45.46	0.229	3.81	0.84	1.74535	0.000147	3.44	3.35	3.52	3.66
33	S0157-33GTV-Tubaf	Fe	42.38	0.279	3.31	0.79	3.6154	0.000275	3.38	3.29	3.39	3.74
34	EPR Sul-fide	Fe	30.11	0.026	2.9	0.7	2.7252	0.000064	3.40	3.21	3.21	3.57
35	S0166-58GTVA-5G	Brec cia	30.18	0.266	3.92	3.07	8201.951	7.07E-05	3.21	3.09	3.25	3.27
36	S0166-70GTVA-2C1	Brec cia	41.42	0.177	2.6	8.33	1100.861	0.000395	3.92	3.89	4.55	4.74
37	M64/1-139GTV-4A7(1)	Brec cia	36.27	0.215	2.62	2.69	795.642	0.032	3.81	3.96	4.10	4.25
38	M64/1-139GTV-4A7(2)	Brec cia	37.91	0.194	2.46	4.05	2790.712	0.0281	3.85	4.06	4.19	4.55
39	M64/1-139GTV-7A2(1)	Brec cia	41.23	0.128	2.96	2.09	5872.975	0.029	3.88	3.73	4.51	4.28
40	M64/1-139GTV-7A2s	Brec cia	33.13	0.246	3.04	2.37	690.9945	0.0154	4.18	4.15	4.31	4.71

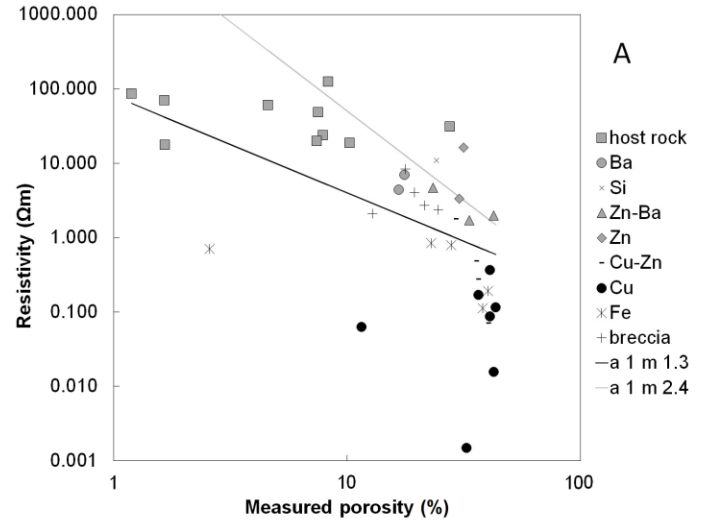

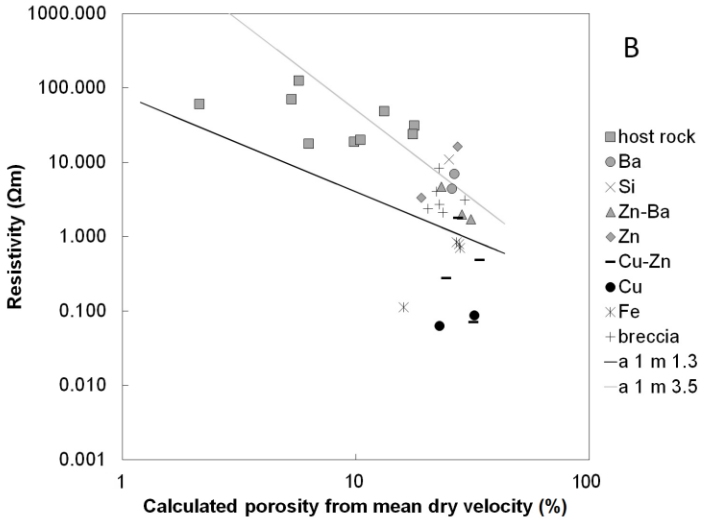

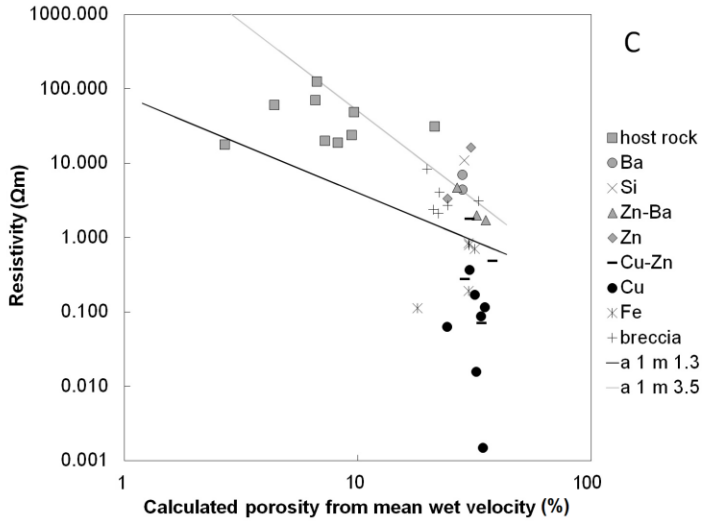

Fig. 9. A) Resistivity vs. porosity. Solid line calculated with Archie's law, *a* = 1 and *m* = 1.3, dashed line *a* = 1 and *m* = 2.4 with fluid resistivity of 0.2 Ωm (modified after Spagnoli et al., 2016c). B) Resistivity vs. mean calculated dry velocity porosity. C) Resistivity vs. mean calculated wet velocity porosity.

From the analysis, we conclude that it is possible during the drilling campaign to measure Vp, and resistivity, as well as magnetic susceptibility to discern mineralized samples, copper and iron rich samples, and host rock *in situ* using the following indicators:

a) Predict porosity based on Vp velocity, and compare whether the predicted resistivity based on Vp derived porosity is observed within the resistivity range
b) If predicted and observed resistivity fall in same range: core samples most likely represent a lower copper/iron grade mineralization.
c) If predicted resistivity is larger than observed resistivity: core samples most likely represent a higher copper/iron grade mineralization.

It is important to note, however, that the tests were performed under atmospheric conditions. At greater depths below the seafloor Ludwig et al. (1998) showed that the porosity will decrease. As drilling operations will be performed to assess the immediate subseafloor of potential massive sulfide occurrences (down to several tens of meters below the seafloor), this influence can likely be neglected here.

4. Conclusions

While SMS offshore and deep-water exploration is currently ongoing, new methods are needed to identify resources while drilling or in recovered core at the drill site. Moreover, borehole data only provide point-source information regarding mineral potential. Thus, it is argued that physical property measurements are needed connecting the formation of sulfide ores and related rock characteristics in these geological settings to the measurable physical properties to validate cross-hole continuity during drilling. P-wave laboratory measurements were carried out on 40 SMS samples from different geological settings. Petrophysical data may provide the necessary link between measurements made at the seafloor and the detection and identification of valuable resources. The results suggest that:

- The Vp velocity is inversely proportional to the porosity and the bulk density, as the increased porosity reduces the elastic moduli of the rock skeleton that decreases Vp.
- Comparing Vp with the electrical resistivity, it is possible to observe that samples with lower velocity have also lower resistivity.
- Considering the correlation of Vp with the magnetic susceptibility, a threshold value separating host from mineralized rock could be set at 4 km/s, where the mineralizations lie below this value.
- Since Vp is controlled mainly by porosity, whereas electrical resistivity is governed by porosity and mineralization, the porosity values were back calculated from Vp and compared with electrical resistivity measurements in order to preliminary assess the presence of mineralization in the cores. Results show that by using Archie's Law, many samples have resistivities more than an order of magnitude below the lower Archie-curve. This can be explained by the presence of a semiconducting material typical in sulfide-rich samples.

Measurements of at least three different physical properties (resistivity, susceptibility and velocity) of SMS samples are important because they allow a preliminary discrimination from host rocks. By combining all the data from Vp, electrical resistivity, and magnetic susceptibility, it is suggested that the non-mineralized specimens have higher velocity (i.e. low porosity), high magnetic susceptibility and low electrical conductivity with respect to the mineralized samples. These findings show promising results regarding the use of geophysical methods for real-time assessment of cores under saturated conditions.

Acknowledgement

The authors would like to thank BAUER Maschinen GmbH for the financial support for this project and for the permission granted to show the results. Thanks also to the anonymous reviewer and to Dr Alireza Malehmir, who considerably increased the quality of the paper. Additionally, we thank Alex Wülbers of the IODP Bremen Core Repository (BCR), and Phil Rumford of the IODP Gulf Coast Repository (GCR) for allowing us to cut the samples using their rock saws.

References

Bellefleur, G., Malehmir, A., Müller, C. 2012. Elastic finite-difference modeling of volcanic-hosted massive sulfide deposits: A case study from Half Mile Lake, New Brunswick, Canada. Geophysics 77, WC25-WC36.

Boschen, R.E., Rowden, A.A., Clark, M.N., and Gardner, J.P.A.,, 2013. Mining of deep-sea seafloor massive sulfides: A review of the deposits, their benthic communities, impacts from mining, regulatory frameworks and management strategies." Ocean Coas. Manag., 84, 54–67.

Bourbié, T., Coussy, O. and Zinszner, B., 1987. Acoustics of Porous Media Gulf Publishing Company.

Brotons, V., Ivorra, S., Tomás, R., Martinéz- Martinéz, J., and Benavante, D,, 2014. Proposal of a new rock creep model. In R. Alejano, A. Perrucho, C. Olalla, and R. Jimenez (Eds.), Rock Engineering and Rock Mechanics: Structures in and on Rock Masses. London: Taylor and Francis Group, pp. 137-141.

Birney, K., Griffin, A., Gwiazda, J., Kefauver, J., Nagai, T. and Varchol, D.,, 2006. Potential deep-sea mining of seafloor massive sulfides: A case study in Papua New Guinea. Donald Bren School of Environmental Science & Management. Available from http://www.bren.ucsb.edu/research/documents/ventsthesis.pdf [cited July 13, 2017].

Cardu, M., and Mucci, A., 2013. Rock Excavation by Drilling and Blasting: Evaluation of the Performance of the Equipment in an Open Pit Limestone Quarry. In C. Drebenstedt and R. Singhal, (Eds.), Mine Planning and Equipment Selection, Springer International Publishing Switzerland, pp. 1127-1142.

Castagna, J.P., Batzle, M.L., and Eastwood, R.L., 1985. Relationships between compressional-wave and shear-wave velocities in elastic silicate rocks. Geophysics 50, 571-581.

Chang, C., Zoback, M.D., Khaksar, A.,, 2006. Empirical relations between rock strength and physical properties in sedimentary rocks. J. Petr. Sci. Eng., 51, 223–237.

Elbra, E., Karlqvist, R., Lasilla, I., Haegström, E. L., and Pesonen, J., 2011. Laboratory measurements of the seismic velocities and other petrophysical properties of the Outokumpu deep drill core samples, eastern Finland. Geophys. J. Int., 184, 405–415.

Hannington, M.D., 2014. Volcanogenic Massive Sulfide Deposits. Treatise on Geochemistry, Vol. 2, pp. 463–488.

Hannington, M.D, De Ronde, C.E., and Petersen, S., 2005. Sea-Floor Tectonics and Submarine Hydrothermal Systems“, Economic Geology 100th Anniversary Volume. J.W. Hedenquist, J. F. H. Thompson, R.J. Goldfarb, and J.P. Richards, (Eds.), Littelton, Society of Economic Geologists, pp. 111-141.

Hannington, M. D., Jamieson, J., Monecke, T., Petersen, S., and Beaulieu, S.,, 2011. The abundance of seafloor massive sulfide deposits. Geology, 39, 1155-1158.

Hördt, A., Bairlein, K., Spagnoli, G., Jegen, M., Hannington, L., Petersen, S. and Laurila, T., 2016. Induced polarization of seafloor massive sulfides. International Workshop on Induced Polarization, Aarhus, Denmark, 6-8 June, 2016.

Gröschel-Becker, H.M., Davis,E.E: and Franklin, J.M., 1994. Data report: Physical properties of massive sulfide from Site 856, Middle Valley, northern Juan de Fuca Ridge. In M.J. Mottl, E.E: Davis, A.T. Fisher and J.F. Slack, (Eds.), Proceedings of the Ocean Drilling Program, Scientific Results, 139. pp. 721-724.

Kassab, M.A., and Weller, A.,, 2015. Study on P-wave and S-wave velocity in dry and wet sandstones of Tushka region. Egypt. Egyptian Journal of Petroleum, 24, 1–11.

Ludwig R.J., Iturrino, G.J., and Rona, P.A.,, 1998. Seismic velocity–porosity relationship of sulfide, sulfate, and basalt samples from the TAG hydrothermal mound. In P.M. Herzig, S.E. Humphris, D.J. Miller and R.A. Zierenberg, (Eds.), Proceedings of the Ocean Drilling Program, Scientific Results, 313-327.

Malehmir, A., Urosevic, M., Bellefleur, G., Juhlin, C., Milkereit, B. 2012. Seismic methods in mineral exploration and mine planning—Introduction. Geophysics 77, 1-2

Malehmir, A., Andersson, M., Lebedev, M., Urosevic, M., Mikhaltsevitch, V. 2013. Experimental estimation of velocities and anisotropy of a series of Swedish crystalline rocks and ores Geophysical prospecting 61, 153-167.

Malehmir, A., Koivisto, E., Manzi, M., Cheraghi, S., Durrheim, R.J., Bellefleur, G., Wijns, C., Hein, K.A.A., King, N. 2014. A review of reflection seismic investigations in three major metallogenic regions:

The Kevitsa Ni–Cu–PGE district (Finland), Witwatersrand goldfields (South Africa), and the Bathurst Mining Camp (Canada). Ore Geology Reviews, 56, 423–441.

Miah, K.H., Bellefleur, G., Schetselaar, E., and Potter, D.K.,, 2015. Seismic properties and effects of hydrothermal alteration on Volcanogenic Massive Sulfide (VMS) deposits at the Lalor Lake in Manitoba, Canada. J. App. Geophys., 123, 141-152.

Miller, S.L.M., and Stewart, R.R.,, 1990. Effects of lithology, porosity and shaliness on P- and S-wave velocities from sonic logs. Canadian Journal of Exploration Geophysics, 26, 1-2, 94-103.

Monecke, T., Petersen, S., Hannington, M.D., Grant, H.,and Samson, I.M.,, 2016.The minor element endowment of modern sea-floor massive sulfides and comparison with deposits hosted in ancient volcanic successions. Reviews in Economic Geology, 18245–306.

Morgan, L.A., 2012. Geophysical characteristics of volcanogenic massive sulfide deposits. In W.C.P. Shanks III, and R. Thurston, (Eds.), Volcanogenic Massive Sulfide Occurrence Model, Reston: US Geological Survey, Reston, VA, pp. 115-131.

Pearce, C. I., Pattrick, R. A., and Vaughan, D. J., 2006. Electrical and magnetic properties of sulfides. Rev. Mineral. Geochem., 61, 127-180.

Petersen, S., Krätschell, A., Augustin, N., Jamieson, J., Hein, J.R. and Hannington, M.D.,, 2016. News from the seabed – Geological characteristics and resource potential of deep-sea mineral resources. Marine Policy, 70, 175–187.

Pridmore, D. F., and Shuey, R. T., 1976. The electrical resistivity of galena, pyrite, and chalcopyrite. Am. Mineral., 61, 248-259.

Rona, P. A., and Scott, S.D., 1993. A Special Issue on Sea-Floor Hydrothermal Mineralization: New Perspectives. Econ. Geol., 88,, 1935-1975.

Saito, S., Ishikawa, M., Arima, M., Tatsumi, Y., 2016. Laboratory measurements of Vp and Vs in a porosity-developed crustal rock: Experimental investigation into the effects of porosity at deep crustal pressures. Tectonophysics, 677–678, 218–226.

Salisbury, M.H., Milkereit, B., Ascough, G., Adair, R., Matthews, L., Schmitt, D.R., Mwenifumbo, J., Eaton, D.W., and Wu, J., 2000. Physical properties and seismic imaging of massive sulfides. Geophysics, 65, 1882-1889.

Schön, J., 2004. Physical properties of rocks - Fundamentals and principles of petrophysics. Elsevier, Amsterdam.

Singer, D.A., 1995. World-class base and precious metal deposits: A quantitative analysis. Econ. Geol., 90, 88–104.

Spagnoli G., Miedema, S.A., Herrmann, C., Rongau, J., Weixler, L. and Denegre, J., 2016a. Preliminary Design of a Trench Cutter System for Deep-Sea Mining Applications Under Hyperbaric Conditions. IEEE J. Ocean. Eng., 41, 930 – 943.

Spagnoli G., Jahn, A., and Halbach, P., 2016b.First results regarding the influence of mineralogy on the mechanical properties of seafloor massive sulfide samples. Eng. Geol., 214, 127–135, http://dx.doi.org/10.1016/j.enggeo.2016.10.007.

Spagnoli G., Hannington, M., Bairlein, K., Hördt, A., Jegen, M., Petersen, S. and Laurila T., 2016c. Electrical properties of seafloor massive sulfides. Geo-Mar. Lett., 36, 235–245.

Spagnoli, G., Hördt, A., Jegen, M., Virgil, C., Rolf, C. and Petersen, S., 2017. Magnetic susceptibility measurements of seafloor massive sulphide mini-core samples for deep-sea mining applications. Q. J. Eng. Geol. Hydroge. 50, 88-93, https://doi.org/10.1144/qjegh2016-113.

Swidinsky, A., Hölz, S., Jegen, M., 2012. On mapping seafloor mineral deposits with central loop transient electromagnetics. Geophysics, 77, E171–E184.

Tufar, W.,, 1991. Paragenesis of complex massive sulfide ores from the Tyrrhenian Sea. Mitteilungen der Österreichischen Geologischen Gesellschaft, 84, 265–300.

Tivey, M.K., 1998. Documenting textures and mineral abundances in minicores from the TAG active hydrothermal mound using X-ray computed tomography. Proceedings of the Ocean Drilling Program, Scientifc Results, 158, 201–210.

Worthington, P. F., 1985. The evolution of Shaly-sand concepts in reservoir evaluation. The Log Analyst, 26, 23-40.

Yamazaki, T., Tomishima, Y., Handa, K., and Tsurusaki, K., 1990. Engineering Properties of Deep-sea Mineral Resources. Proceedings 4th Pacific Congress on Marine Science and Technology, pp. 385-392.

Yamazaki, T., and Park, S.H., 2003. Relationship between Geotechnical Engineering Properties and Assay of Seafloor Massive Sulfides. Proc. 13th International Offshore and Polar Eng. Conference Honolulu, pp. 310-316.

Zhu, W., Tivey, M.K., Gittings, H. and Craddock, P.R., 2007. Permeability-porosity relationships in seafloor vent deposits: Dependence on pore evolution processes. Journal of Geophysical Research, 112, B05208, doi:10.1029/2006JB004716.

FIGURE CAPTIONS

Fig. 1. Location of the sample used for the laboratory experiments.

Fig. 2. Rock saws used at the BCR for making precise and parallel cuts. A) standard IODP single 10-inch blade rock saw, and B) ASC Scientific Dual Blade rock saw.

Fig. 3. Principle setup for ultrasonic P-wave velocity measurements.

Fig. 4. Examples of first arrivals used to calculate the velocities for the dry and wet ultrasonic measurements. A) Sample S0166 59 GTVA-1B1 (chimney Zn-Ba) showing a strong signal for both dry (5.44 µs) and wet (5.16 µs) first arrivals. B) Sample S0208 DR100-3A (chimney Zn) showing no signal for the dry measurement, and a weak signal for the wet (1.54 µs) first arrival. The cutoff of the crosstalk signal from the high voltage transmitter pulse illustrates the high amplification of the record.

Fig. 5. Comparison plots of dry (A), and wet (B) velocity measurements vs. porosity. Note: data points that lie on the x-axis in (A) represent samples with no signal and distinguishable first arrivals.

Fig. 6. Comparison plots of dry (A), and wet (B) velocity measurements vs. bulk density. Note: data points that lie on the x-axis in (A) represent samples with no signal and distinguishable first arrivals.

Fig. 7: 3D plot of velocity, resistivity and magnetic susceptibility (the latter are from Spagnoli et al., 2016c and 2017). In comparison to basalt host rock, mineralized cores exhibit lower resistivity, higher velocities and higher susceptibilities. The red color for the Ba samples means negative SI values.

Fig. 8. Comparison between calculated porosity from Vp measurements on wet samples and measured porosity.

Fig. 9. A) Resistivity vs. porosity. Solid line calculated with Archie's law, a = 1 and m = 1.3, dashed line a = 1 and m = 2.4 with fluid resistivity of 0.2 Ωm (modified after Spagnoli et al., 2016c). B) Resistivity vs. mean calculated dry velocity porosity. C) Resistivity vs. mean calculated wet velocity porosity.

Highlight

- It is important to develop systems able to detect and classify mineralized zones from waste materials while drilling deep-water;
- Seismic P-wave velocities (Vp) were measured on 40 SMS and unmineralized mini-cores;
- The porosity was back-calculated from Vp;
- The results were compared with electrical resistivity measurements;
- Using Archie's Law, it is possible to observe that metallic conduction exists.